Journal of Intelligent & Robotic Systems (2022) 104: 23
https://doi.org/10.1007/s10846-021-01533-9

REGULAR PAPER

AUV Path Planning Based on Differential Evolution with Environment Prediction

Jiaxin Zhang[1,2] · Meiqin Liu[1,3] · Senlin Zhang[2] · Ronghao Zheng[2]

Received: 24 June 2021 / Accepted: 23 September 2021 / Published online: 22 January 2022

Abstract

Energy-efficient path planning is essential for the autonomous underwater vehicle (AUV)-based ocean exploration. Existing static environment-based AUV path planners do not work well in dynamic ocean environments. A novel onboard sensing system-based AUV path planning strategy is proposed, and it is suitable for a regional dynamic environment to improve the energy utilization efficiency of an AUV working in a small-scale and dynamic mission area. Firstly, unlike the existing methods, the onboard sensing system including horizontal acoustic doppler current profile and detecting sonar is used to obtain environmental information, and the probabilistic multiple hypothesis tracker and Kalman filter are employed to carry out multi-step prediction of the environment. After that, the differential evolution algorithm is introduced as the optimizer, and a novel prediction-based path evaluator is designed to evaluate the fitness of possible paths. Besides, a novel prediction-based online re-planning strategy is designed, which is beneficial to reduce the impact of forecast error and the planning is thus closed-loop. Finally, multiple simulation experiments are designed to verify the effectiveness and superiority of the path planner, and the results show that the proposed planning strategy can reduce the AUV energy consumption by at least 4.6% compared with static environment-based planners.

Keywords Autonomous underwater vehicle · Kalman filter · Dynamic environment · Path planning

1 Introduction

Due to the high mobility and sensors integration, the autonomous underwater vehicle (AUV) is playing a non-negligible role in many fields, such as marine expedition, aquaculture, data collection, and industrial devices monitoring [1]. The ocean environment is full of complexities and vagaries, so the AUV should autonomously plan its path to avoid collisions and save the battery energy by utilizing the ocean current. It is challenging for an AUV to reach a satisfactory path in the mission region with the existence of dynamic obstacles and time-varying current, which may seriously endanger driving safety and impact AUV's duration [2].

Path planning techniques are well-studied up to now, and the fruitful progress can be applied to the further study of AUV path planning. Geometric model search algorithms that belong to the discrete optimal programming are classical path search algorithms. Many of them have been improved for AUV path planning, such as Dijkstra algorithm [3], A* algorithm [4], the fast marching (FM) algorithm [5], and level set method (LSM) [6]. The low efficiency of the above geometric model-based algorithms when being applied to a large-scale complex underwater environment is still a fatal shortcoming [7]. The rapidly exploring random tree (RRT) algorithm is powerful in spatial searching, and experiments utilizing improved RRT on three-dimensional path planning for an AUV in real sea areas have achieved satisfactory results [8]. Although the

✉ Meiqin Liu
liumeiqin@zju.edu.cn

Jiaxin Zhang
zhangjiaxin@zju.edu.cn

Senlin Zhang
slzhang@zju.edu.cn

Ronghao Zheng
rzheng@zju.edu.cn

[1] The State Key Laboratory of Industrial Control Technology, Zhejiang University, Hangzhou, 310027, China

[2] College of Electrical Engineering, Zhejiang University, Hangzhou, 310027, China

[3] The Institute of Artificial Intelligence and Robotics, Xi'an Jiaotong University, Xi'an, 710049, China

search speed is fast, the result given by RRT or its variants are usually suboptimal, and it is difficult to find a practical path in a narrow channel [9].

Besides the geometric-based algorithms mentioned above, intelligence algorithms that are efficient and robust in complex environments have attracted more and more attention [10]. Typical intelligent algorithms for path planning include the particle swarm optimization algorithm (PSO) [11, 12], the ant colony optimization algorithm (ACO) [13], and the genetic algorithm (GA) [14]. Besides, the differential evolution (DE) algorithm, which is an improved version of the GA, was used in both local and global AUV path planning [15]. A common weakness of all intelligence algorithms is the large computational consumption. However, [16] proved that the searching speed of swarm intelligence path planning algorithms can be satisfied by adopting the field-programmable gate array (FPGA)-based parallel computing strategy. Reliable optimization capability and real-time performance enhance the advantages of intelligence algorithms in AUV path planning.

The dynamic environment containing strong ocean current is always out of consideration [3]. It is admitted that the impact of ocean currents on AUV's motion is not always significant [17], but this effect is non-negligible in many cases. Inadequate consideration of the dynamic of the current may result in the deterioration of the planned path's optimality because of the change of the environment during AUV's operation [18, 19]. Many attempts were made to deal with the path planning problem in time-varying currents field, but it is still full of challenges to predict ocean current given the predictive capabilities of present modeling systems. The problem of current prediction was solved to a certain extent on the basis of global real-time ocean forecast system (RTOFS-Global) and navy coastal ocean model (NCOM), which are predictive tools used in open-source ocean modeling [12]. However, in many mission scenarios, such as exploration around the island and monitoring in marine pastures, the AUV works in a small-scale region, which is often within tens of kilometers, and the numerical forecast models are seldom helpful in estimating and predicting the environment in these situations [20]. Horizontal acoustic doppler current profile (H-ADCP) is believed to be helpful to infer the two-dimensional structure of the current field in a limited region in front of the AUV [21]. The regional current field can be parameterized by approximating the solution of two-dimensional Navier-Stokes equation as the superposition of one-point vortex solutions called viscous Lamb vortexes [22]. However, this method needs to be extended to be suitable for path planning in the spatiotemporal current. Besides, another important problem is to avoid collisions with dynamic obstacles during AUV's operation. The path planning algorithms mentioned above can only deal with planning problems in static environments and have to be combined with a dynamic obstacle avoidance system, which results in frequent unplanned maneuvers, and the optimal path in a complex environment is hence often hard to achieve.

Based on AUV onboard sensors, we aim to design an AUV path planning method which can utilize ocean current energy and avoid obstacles more efficiently, and consequently enhance the durability of the AUV working in a small-scale mission region. Usually, there are a series of tasks to be carried out by the AUV during one launch. The path planning strategy reduces the energy consumption of each task effectively to achieve the purpose of completing as many tasks as possible in one voyage. The essential structure of our path planner is illustrated in Fig. 1. The main contributions conclude:

- Based on the measurements obtained by H-ADCP and detecting sonar, the Kalman filter (KF) is used to obtain the multi-step prediction of the future states of ocean current and dynamic obstacles.
- The DE algorithm is employed as the optimal path searcher, and any possible path generated by it is evaluated based on the prediction of the environment.
- The environment is re-sensed during the AUV's movement to correct the multi-step prediction. After that, the re-planning mechanism is introduced to maintain the optimality of the subsequent path.

The rest of this paper is organized as follows. Section 2 describes the mathematical model of the AUV path planning problem and environment model. Section 3 introduces the DE algorithm and the environment prediction method used

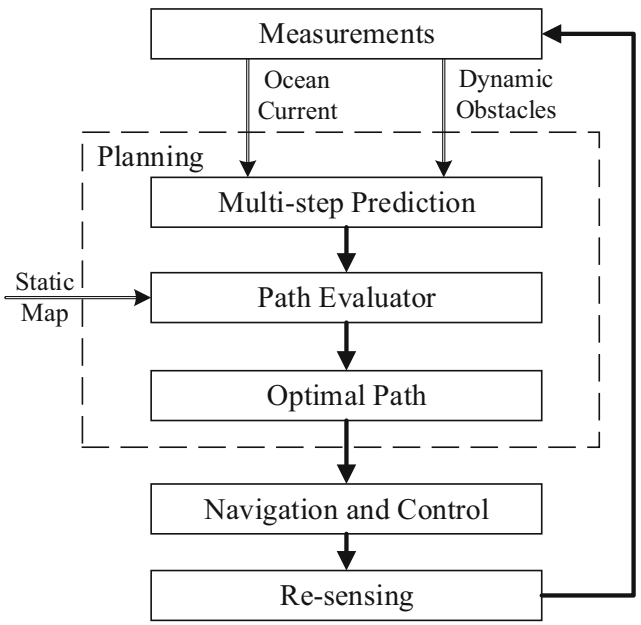

Fig. 1 Structure of the introduced Path Planner

in path planning. Section 4 gives the re-sensing-based re-planning strategy. In Section 5, the simulation set and results of comparisons are discussed. Section 6 draws the conclusion.

2 Problem Formulation

2.1 AUV's Mission and Path Evaluation

In a single mission, the AUV starts at the starting point and moves toward the destination. The path planning system is supposed to screen out the optimal path P^* from the possible path set $\boldsymbol{P}$. By following P^*, the AUV accomplishes its motion at the lowest energy cost, and the possibility of collision is minimized. A sample of such a mission is depicted by Fig. 2.

The problem of AUV's path planning is considered as an optimization problem, and it is reasonable to take energy consumption as the optimization goal function. Because of the proportion between the water-referenced velocity and the cube root of the thrust, the AUV's thrust power is constant, and then it is reasonable to assume that the AUV's water-referenced velocity is constant for simplicity [12]. In other word, we assume the AUV adopts an accurate enough motion controller to adjust its attitude in real time according to the given path. Consequently, the time consumption, which is a constant multiple of energy consumption, is adopted to be the optimization function.

The AUV departs from $\boldsymbol{A}(x_0, y_0, z_0)$ and is hoped to arrive at $\boldsymbol{B}(x_n, y_n, z_n)$. $P = \{\boldsymbol{p}_0, \ldots, \boldsymbol{p}_i, \ldots, \boldsymbol{p}_n\}$ is one feasible path, where $\boldsymbol{p}_i(x_i, y_i, z_i)(0 \leq i \leq n)$ are way points of the path. AUV's ground-referenced velocity $\boldsymbol{V}_g$ is the resultant of the water velocity $\boldsymbol{V}_c$ and its constant water-referenced velocity $\boldsymbol{V}_a$, satisfying

$$\boldsymbol{V}_g = \boldsymbol{V}_a + \boldsymbol{V}_c \tag{1}$$

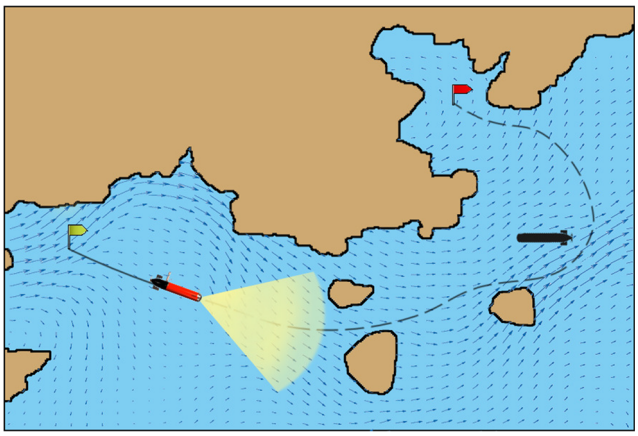

Fig. 2 An AUV following the planned path in the mission region

where the direction of $\boldsymbol{V}_g$ is the same as the tangent of the path, as shown in Fig. 3. The AUV's ground-referenced velocity can be derived by the digital visual interface (DVL) [23] in real time.

A feasible path satisfies

$$P \cap \{\boldsymbol{O}, \boldsymbol{L}\} = \emptyset \tag{2}$$

where $\boldsymbol{O}$ is obstacles in the operation ocean area and $\boldsymbol{L}$ is land, which means there exists no possible collision, and

$$\frac{\boldsymbol{V}_g}{|\boldsymbol{V}_g|} = \frac{\boldsymbol{p}_{i+1} - \boldsymbol{p}_i}{|\boldsymbol{p}_{i+1} - \boldsymbol{p}_i|} \tag{3}$$

which means the AUV will not be caught by strong counter-currents and can keep moving forward.

The time consumption of the path, which is meanwhile the objective function J, is given by

$$\begin{aligned} J(P) = t_{sum} &= \sum_{i=1}^{n} t_i \\ &= \sum_{i=1}^{n} \frac{|\boldsymbol{p}_{i+1} - \boldsymbol{p}_i|}{|\boldsymbol{V}_{g,i}|} \end{aligned} \tag{4}$$

where $\boldsymbol{V}_{g,i}$ is the ground-referenced velocity of the AUV in the segment path $\{\boldsymbol{p}_i, \boldsymbol{p}_{i+1}\}$. $\boldsymbol{p}_i$ and $\boldsymbol{p}_{i+1}$ are adjacent way points in the path. Notice that to make the calculation feasible, approximate discretization is performed. Equation 4 suggests that the local current influences the time cost of $\{\boldsymbol{p}_i, \boldsymbol{p}_{i+1}\}$. Thus, the AUV should take advantage of the ocean current to minimize the total time consumption.

The purpose of the path planning is formulated as the following optimization problem:

$$\begin{aligned} P^* &= \arg\min_{P \in \boldsymbol{P}} J(P) \\ &= \arg\min_{P \in \boldsymbol{P}} t_{sum} \\ &= \arg\min_{P \in \boldsymbol{P}} \sum_{i=1}^{n} \frac{|\boldsymbol{p}_{i+1} - \boldsymbol{p}_i|}{|\boldsymbol{V}_{g,i}|} \end{aligned}$$

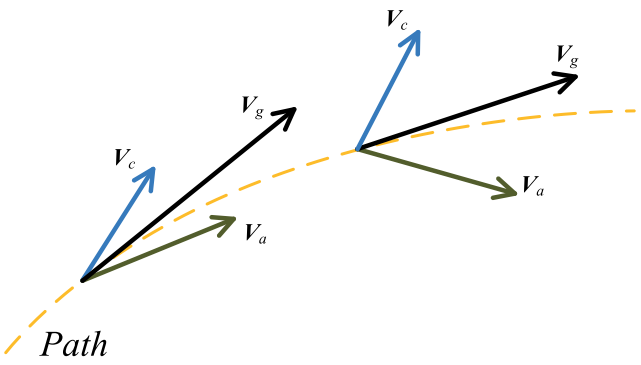

Fig. 3 Ground-referenced velocity V_g: resultant of current velocity V_c and thrust velocity V_a

$$
\begin{aligned}
s.t.\ \ & \boldsymbol{p}_0 = \boldsymbol{A}(x_0, y_0, z_0), \\
& \boldsymbol{p}_n = \boldsymbol{B}(x_n, y_n, z_n), \\
& \boldsymbol{\mathcal{M}}_{AUV} = 0
\end{aligned} \tag{5}
$$

where $\boldsymbol{\mathcal{M}}_{AUV}$ is AUV's kinematic model [24], which means sharp curves are undesired during the planning. In addition to this, the planning method is independent of the AUV model.

2.2 No-fly Zone: Land and Obstacles

In most cases, the mission region is not completely free for a sail because of the existence of land $\boldsymbol{L}$ and obstacles $\boldsymbol{O}$ [25]. Because the safety of AUV is always the top priority, a feasible path should avoid any possible collision. That is, no intersection is allowed between P and $\{\boldsymbol{L}, \boldsymbol{O}\}$. The AUV's only changes its depth on the beginning navigation stage, which means its depth is almost constant after starting the movement. Besides, the AUV's vertical motion is comparatively negligible due to large horizontal scales [15], and the AUV's motion is usually assumed to be on a horizontal plane. Thus, all the operations in our research are performed on the two-dimensional horizontal plane.

The land $\boldsymbol{L}$ includes coasts, reefs, and islands. It is prior information which can be obtained by satellite imagery and manual measurement. Related technologies are mature enough to convert satellite images or artificial charts into 0-1 maps, in which 1 stands for the accessible area and 0 stands for the no-fly zone. The map marking out the land is sent to the vehicle before departure. Static obstacles, such as fishing cages and other artificial facilities, can also be treated in the same way.

The mission region is always close to busy ports or fisheries, where vessels and sampans are common. Besides, other AUVs and fish schools will also bring danger. These moving objects which introduce uncertainty to AUV's safety are defined as dynamic obstacles, and the AUV has to handle them automatically. For those dynamic obstacles that can not be detected in advance, AUV uses vehicle-borne sonars to locate and track them. These obstacles act autonomously in most cases, so the impact of ocean current on them can be ignored. Based on this, a dynamic obstacle is considered as a mass point moving at constant velocity (CV) in a period, and its position uncertainty is modeled as an independent Gaussian distribution [26], and the process noise compensates the possible changes in target velocity [27]. Ignoring the vertical position change, the state of obstacle o at time k can be written as $\boldsymbol{x}_o(k) = \left[x(k), v_x(k), y(k), v_y(k)\right]_o^T$. Hence the formulation of the motion satisfies

$$
\boldsymbol{x}_o(k) = \boldsymbol{F}_{CV}\boldsymbol{x}_o(k-1) + \boldsymbol{w}_p(k) \tag{6}
$$

where $\boldsymbol{F}_{CV}$ is the state transition matrix and $\boldsymbol{w}_p(k)$ is the process noise with zero-mean white Gaussian distribution $\mathcal{N}(0, \boldsymbol{Q}(k))$. $\boldsymbol{F}_{CV}$ and $\boldsymbol{Q}(k)$ are given by

$$
\boldsymbol{F}_{CV} = \begin{bmatrix} 1 & T & 0 & 0 \\ 0 & 1 & 0 & 0 \\ 0 & 0 & 1 & T \\ 0 & 0 & 0 & 1 \end{bmatrix}, \boldsymbol{Q}_k = q^2 \begin{bmatrix} \frac{T^3}{3} & \frac{T^2}{2} & 0 & 0 \\ \frac{T^2}{2} & T & 0 & 0 \\ 0 & 0 & \frac{T^3}{3} & \frac{T^2}{2} \\ 0 & 0 & \frac{T^2}{2} & T \end{bmatrix} \tag{7}
$$

where q is the intensity of the process noise of the CV model and T is the sample interval [28].

Areas where the dynamic obstacles appear are marked as "no-fly zone" together with the land and static obstacles. To avoid the collision brought by position uncertainty, we define the no-fly zone caused by o as a circle with the peak of position distribution S_o being the center, and the radius R satisfies

$$
P(||S_o - S_r|| < R) = 1 - \eta \tag{8}
$$

where S_r is the obstacle's real position and η is the maximum tolerable collision probability. For instance, if $\eta = 0.01$, the circle with radius R represents the collision boundary with the confidence of 99%.

2.3 Time-varying Current

The ocean currents may influence the AUV positively or negatively. The vehicle saves much energy flowing downstream and consumes additional energy when going upstream. The AUV may even get caught in the vortex if the current is too strong. The ocean dynamics can be described by the 2-D Navier-Stokes equation:

$$
\frac{\partial \omega}{\partial t} + (\boldsymbol{V}\nabla)\omega = \nu \Delta \omega \tag{9}
$$

where $\boldsymbol{V} = (V_x, V_y)$ is the ocean current velocity field, ν is the viscosity of the ocean, ω is the vorticity and ∇ and Δ are respectively the gradient and Laplacian operators. In consideration of simplicity and timeliness of the calculation, it is impossible to handle such an equation that is difficult to be solved analytically online by using the finite element method. Fortunately, the current field can be modeled as a superposition of multiple Lamb vortexes [21]. The current velocity at $\boldsymbol{r}(x, y)$ in the field excited by a single vortex can be expressed as

$$
\begin{aligned}
& \boldsymbol{V}_c = (v_{c,x}, v_{c,y}) = f(\boldsymbol{r}_0(x_0.y_0), \Gamma, \delta) \\
& v_{c,x} = -\Gamma \frac{y - y_0}{2\pi(\boldsymbol{r} - \boldsymbol{r}_0)^2}\left[1 - e^{\frac{-(\boldsymbol{r}-\boldsymbol{r}_0)^2}{\delta^2}}\right] \\
& v_{c,y} = \Gamma \frac{x - x_0}{2\pi(\boldsymbol{r} - \boldsymbol{r}_0)^2}\left[1 - e^{\frac{-(\boldsymbol{r}-\boldsymbol{r}_0)^2}{\delta^2}}\right]
\end{aligned} \tag{10}
$$

where $\boldsymbol{r_0}(x_0, y_0)$ is the vortex center, $v_{c,x}$ and $v_{c,y}$ are respectively the two horizontal components of the current velocity $\boldsymbol{V}_c$, Γ is the vortex strength, and δ is the vortex radius. Equation 10 describes the static current field in the ocean, but the current is generally time-varying in the mission region. When a vortex is not close to another, it will move with nearly uniform velocity in the direction of its rectilinear axis [22]. Therefore, the vortex can also be described by CV model and the parameters of the dynamic vortex at time k can be determined by

$$\boldsymbol{x}_v(k) = \boldsymbol{F}_{CV}\boldsymbol{x}_v(k-1) + \boldsymbol{w}_p(k) \tag{11}$$

where $\boldsymbol{x}_v(k) = \left[x(k), v_x(k), y(k), v_y(k)\right]_v^T$ is the state of the vortex, $\boldsymbol{F}_{CV}$ and $\boldsymbol{w}_p(k)$ are respectively the state transition matrix and process noise defined by Eq. 7.

3 DE-based Path Planning with Prediction of the Environment

A path planner's duty is to find a feasible path by following which the AUV can take full advantage of current, avoid collisions, and save as much energy as possible. Since the AUV's motion is coupled to the environment, the credible estimation of the time-varying current and moving obstacles is meaningful.

Planners based on swarm or evolutionary algorithms have been proved to be feasible and efficient in AUV path planning [29]. DE is one of the most powerful and versatile evolutionary optimizers for the continuous parameter spaces, and it has exhibited remarkable performance in terms of final accuracy, computational speed, and robustness [30]. Figure 4 presents the structure of the proposed DE-based path planner.

3.1 DE-based AUV Path Planner

3.1.1 Chromosome and Coding

The details of a path are decided by r control points. Given the starting point and the destination, the line segments that connect these points in sequence constitute the basic path. Naturally, the basic path has to be smoothed to form a feasible path, and that would be discussed latter.

Two real numbers are used to represent the two horizontal coordinates of each one of the r control points in the 2-D space. Thus the chromosome $\boldsymbol{C}_i$ of individual i contains $2r$ genes

$$\boldsymbol{C}_i = \left[x_{i,1}, x_{i,2}, \ldots, x_{i,r}, y_{i,1}, y_{i,2}, \ldots, y_{i,r}\right]^T. \tag{12}$$

The genetic operations described later will be performed on the chromosomes of each individual in the population.

3.1.2 Evolutionary Operations

The DE algorithm is made up of the following four basic steps:

- Initialization: Assume the size of the population is n. Generate n individuals with the elements of whose chromosomes are randomly selected in the 2-D mission region.
- Mutation: For $\boldsymbol{c}_i^t$, the i-th individual in generation t, create the donor vector with

$$\boldsymbol{v}_i^t = \boldsymbol{c}_i^t + F \times \left(\boldsymbol{c}_p^t - \boldsymbol{c}_q^t\right), \tag{13}$$

where F is the scaling factor, and $\boldsymbol{c}_p^t$ and $\boldsymbol{c}_q^t$ are two different individuals who are chosen randomly from the population.

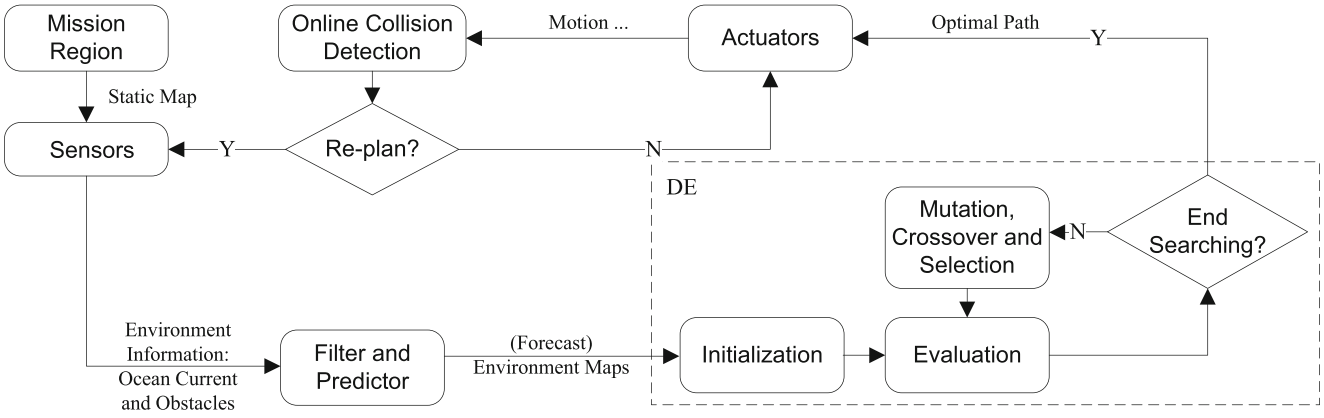

Fig. 4 DE-based Path Planning with Forecast Environment Map

– Crossover: The donor vector $\boldsymbol{v}_i^t$ will be mixed with $\boldsymbol{c}_i^t$ to form the offspring $\boldsymbol{u}_i^t$ according to

$$u_{i,j}^t = \begin{cases} v_{i,j}^t & rand_{i,j}[0,1] < K \\ c_{i,j}^t & rand_{i,j}[0,1] \geq K \end{cases} \tag{14}$$

where $u_{i,j}^t$ is the j-th gene of $\boldsymbol{u}_i^t$, and K is the crossover rate predefined.

– Selection: The selection operator determines whether the chromosome $\boldsymbol{u}_i^t$ generated by mutation and crossover will survive to the next generation. The i-th individual in the $(t+1)$th generation will be

$$\boldsymbol{c}_i^{t+1} = \begin{cases} \boldsymbol{u}_i^t & J\left(\boldsymbol{u}_i^t\right) < J\left(\boldsymbol{c}_i^t\right) \\ \boldsymbol{c}_i^t & J\left(\boldsymbol{u}_i^t\right) \geq J\left(\boldsymbol{c}_i^t\right). \end{cases} \tag{15}$$

By performing the above operations on each individual in the population (except initialization, which is only for the 1st generation), individuals in the next generation are determined.

3.1.3 Path Smoothing

A smooth curve is more feasible for the AUV to follow than a couple of straight lines. Thus B-spline method [31] is employed to smooth the path determined by the chromosome-defined m control points. The B-spline smoother is integrated into the path planner. Specifically, the smoother is called to produce the corresponding feasible curve every time when a new chromosome is generated. The time consumption of the smoothed path will be used in the following evaluation and evolution. The path defined by an individual and the B-spline curve based on it is depicted by Fig. 5.

3.2 Forecast Dynamic Environment with Kalman Predictor

The AUV detects the external environment using onboard sensors. The detecting sonar system is powerful in detecting the position and motion of obstacles over the range of hundreds of meters [32], and H-ADCP is believed to be effective in inferring the two-dimensional structure of the current field within 300 meters ahead the vehicle [21]. The current environmental information obtained by the sensing system is helpful in path planning. However, if the planner plans the path only on the basis of the current external environment, the variation of the environment will definitely weaken the practice performance of the result.

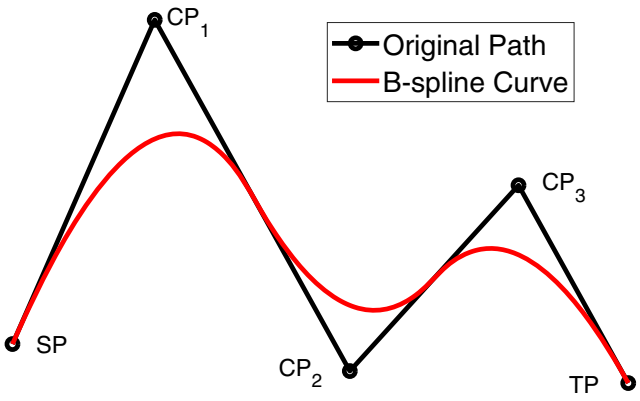

Fig. 5 Control points and B-spline curve

From the one-dimensional information obtained from an H-ADCP, Ref. [21] provided a practical algorithm to abstract parameters (vortexes center, strength, and radius) of the current made up of several vortexes. The vortex parameters, together with the positions and velocities of obstacles, constitute the state vector to be estimated and forecast. That is, state vector at time k is defined as

$$\boldsymbol{x}(k) = \{\boldsymbol{x}_v(k); \boldsymbol{x}_o(k)\} \tag{16}$$

and the measurements are obtained by

$$z(k) = \boldsymbol{H}\boldsymbol{x}(k) + \boldsymbol{w}_o(k) \tag{17}$$

where $\boldsymbol{H}$ is the output matrix and $\boldsymbol{w}_o(k)$ is the observation noise superimposed on the outputs. For simplicity, $\boldsymbol{H}$ is chosen to be identity matrix and $\boldsymbol{w}_o(k)$ is Gaussian noise.

For a single moving target, KF is a powerful tool to estimate and predict its state [33]. It is requisite to associate multiple measurements with their sources if we want to predict the future state of the environment that contains multiple vortexes and obstacles. In the open ocean environment, it is usually easy to distinguish measurements of different moving objects, and the similar property of vortexes is stated in Section 2.3. In our work, the expectation-maximization-based probabilistic multi-hypothesis tracker (PMHT) [34] is employed to carry out the measurement-association task.

Here we take the obstacle detecting system as an example. The number of obstacles in the field of sonar scope is dynamic, and the adjustment of it can be accomplished by employing existing track initiation and termination methods, such as the logic-based technique [35].

Assume there are n_o obstacles existing at a certain stage of the sensing, and m_o measurements are detected. The measurements can be effectively associated with the obstacles by carrying out the PMHT algorithm. The result of the association can be converted from the probabilistic form to the definite form by applying

$$f_k(i,j) = \underset{s\in[1,n_o]}{\arg\max}\, \pi_k^s,\ (1 \leq i \leq m_o, 1 \leq j \leq n_o) \tag{18}$$

where $f_k(i,j) = s$ means the j-th measurement at time k comes from obstacle s, and π_k^s is the probability that the measurement comes from the obstacle s. The problem is consequently converted into several single-target prediction problems.

Multi-step prediction [36] is performed to forecast the future state of the obstacle. Consider the system described by Markov model:

$$\begin{cases} \boldsymbol{x}(k+1) = \boldsymbol{\Phi}(k+1,k)\boldsymbol{x}(k) + \boldsymbol{B}(k+1,k)\boldsymbol{w}(k) \\ \boldsymbol{z}(k+1) = \boldsymbol{H}(k+1)\boldsymbol{x}(k+1) + \boldsymbol{v}(k+1) \end{cases} \tag{19}$$

where $\boldsymbol{\Phi}(k+1,k)$ is one-step state transition matrix, $\boldsymbol{B}(k+1,k)$ is excitation transition matrix, $\boldsymbol{w}(k) \sim \mathcal{N}(0, \boldsymbol{Q}(k))$ is process noise, $\boldsymbol{H}(k+1)$ is output matrix, and $\boldsymbol{v}(k+1) \sim \mathcal{N}(0, \boldsymbol{R}(k+1))$ is observation noise. The optimal prediction with the advanced-time N is

$$\hat{\boldsymbol{x}}(k+N|k) = \boldsymbol{\Phi}(k+N,k)\hat{\boldsymbol{x}}(k|k) \tag{20}$$

where

$$\boldsymbol{\Phi}(k+N,k) = \prod_{i=k}^{k+N-1} \boldsymbol{\Phi}(i+1,i) \tag{21}$$

is the N-step state transition matrix, and $\hat{\boldsymbol{x}}(k|k)$ is the optimal state estimation at time k.

The performance of the prediction is described by error covariance

$$\begin{aligned} \boldsymbol{P}(k+N|k) = {} & \boldsymbol{\Phi}(k+N,k)\boldsymbol{P}(k|k)\boldsymbol{\Phi}^T(k+N,k) \\ & + \sum_{i=k+1}^{k+N} \Big[\boldsymbol{\Phi}(k+N,i)\boldsymbol{B}(i,i-1)\boldsymbol{Q}(i-1) \\ & \times \boldsymbol{B}^T(i,i-1)\boldsymbol{\Phi}^T(k+N,i)\Big] \end{aligned} \tag{22}$$

where $\boldsymbol{Q}(k)$ is the covariance of $\boldsymbol{w}(k)$.

For the obstacle system with $\boldsymbol{x} = [x, y, v_x, v_y]^T$ being the state vector, $\boldsymbol{B}(k+1,k) = \boldsymbol{I}$ is unit matrix, $\boldsymbol{\Phi}(k+1,k)$ is time-independent, and $\boldsymbol{w}(k)$ is Gaussian noise. Thus the error covariance is

$$\begin{aligned} \boldsymbol{P}(k+N|k) = {} & \boldsymbol{\Phi}^N \boldsymbol{P}(k|k) \left(\boldsymbol{\Phi}^T\right)^N \\ & + \sum_{i=k+1}^{k+N} \left[\boldsymbol{\Phi}^{k+N-i} \boldsymbol{Q} \left(\boldsymbol{\Phi}^T\right)^{k+N-i}\right]. \end{aligned} \tag{23}$$

For an obstacle moving in CV mode, $\boldsymbol{F}^{CV}$ given by Eq. 7 is substituted in Eq. 23, therefore

$$\begin{aligned} \boldsymbol{P}(k+N|k) = {} & \boldsymbol{F}_{CV}^N \boldsymbol{P}(k|k) \left(\boldsymbol{F}_{CV}^T\right)^N \\ & + \sum_{i=k+1}^{k+N} \left[\boldsymbol{F}_{CV}^{k+N-i} \boldsymbol{Q} \left(\boldsymbol{F}_{CV}^T\right)^{k+N-i}\right]. \end{aligned} \tag{24}$$

It is well known that elements on the main diagonal of $\boldsymbol{P}(k+N|k)$ indicate the uncertainty of the state prediction of time $k+N$. Subsequently, the forecast map of the no-fly zone can be generated according to Eq. 8.

The state vector of the ocean vortex system is

$$\boldsymbol{x} = \left[\boldsymbol{x}_c, \boldsymbol{y}_c, \boldsymbol{v}_x, \boldsymbol{v}_y, \boldsymbol{\Gamma}, \boldsymbol{\delta}\right]^T \tag{25}$$

where $\boldsymbol{x}_c$ and $\boldsymbol{y}_c$ are positions of vortexes' centers. The current measurements and the vortexes can also be uncoupled by using the PMHT algorithm. Then Eqs. 20 - 24 are employed to carry out the prediction. The ocean current field can be constructed by substituting the forecast parameters in Eq. 10.

The predictor can give out the predictions of the next N sampling periods. The obstacle map and current map together form the forecast map to be used to evaluate paths.

3.3 Path Evaluation Using Forecast Map

In the DE-based path planner, multiple individuals corresponding to different paths are generated in each generation. The predictions of the environment given in Section 3.2 will be used in path evaluation, and the results are used as the gist in the subsequent evolution.

Now we consider path $P = \{\boldsymbol{p}_0, \boldsymbol{p}_1, \ldots, \boldsymbol{p}_n\}$. The sample interval is T_s, and the forecast environment map series given by the predictor is $\boldsymbol{M}_f = \{M_1, M_2, \ldots, M_N\}$. That is, $\boldsymbol{M}_f$ contains the predictions for the next N periods.

As what Eq. 4 states, traveling time is chosen to be the optimization goal. Thus

$$J = t_{sum} = \sum_{i=0}^{n-1} t_i \tag{26}$$

where t_i satisfies

$$t_i = \frac{|\boldsymbol{p}_{i+1} - \boldsymbol{p}_i|}{|\boldsymbol{V}_g|} = \frac{|\boldsymbol{p}_{i+1} - \boldsymbol{p}_i|}{|\boldsymbol{V}_a + \boldsymbol{V}_c|}. \tag{27}$$

When calculating t_i, the proposed evaluator uses the forecast map $M_{[T_i]}$ instead of the static environment map, and

$$T_i = \frac{1}{T_s} \sum_{j=1}^{i-1} t_j + 1 \tag{28}$$

is the time cost of sub-path $\{\boldsymbol{p}_1, \boldsymbol{p}_2, \ldots, \boldsymbol{p}_i\}$, which is the first part of P, and $[T_i]$ is the integer part of T_i. The estimator accumulates the time cost of each segment of the path from the starting point, and calls the next frame prediction map whenever the threshold is reached, i.e., $[T_i]$ is changed. To put it more clear, Eq. 26 can be transformed into

$$\begin{aligned} t_{sum} = {} & \underbrace{t_1 + \cdots + t_a}_{M_1} + \underbrace{t_{a+1} + \cdots + t_b}_{M_2} \\ & + \cdots + \underbrace{t_c + \cdots + t_{n-1}}_{M_q} \quad (q \le N) \end{aligned} \tag{29}$$

where M_q is the last forecast map in $\boldsymbol{M}_f$ that is used until the AUV arrives at the destination or the re-plan is performed.

Many paths generated by DE may cross the no-fly zone or strong counter-current area, but the above calculation does not consider the feasibility of the path. Thus, the feasible detection should be performed.

For path P, after the time cost of $[\boldsymbol{p}_i, \boldsymbol{p}_{i+1}]$ is obtained, define the feasible detection mark

$$F_i = \begin{cases} 0 & [\boldsymbol{p}_i, \boldsymbol{p}_{i+1}] \cap \{\boldsymbol{O}, \boldsymbol{L}\} \neq \emptyset \text{ or } \frac{\boldsymbol{V}_g}{|\boldsymbol{V}_g|} \neq \frac{\boldsymbol{p}_{i+1}-\boldsymbol{p}_i}{|\boldsymbol{p}_{i+1}-\boldsymbol{p}_i|} \\ 1 & \text{others} \end{cases} \tag{30}$$

where $[\boldsymbol{p}_i, \boldsymbol{p}_{i+1}] \cap \boldsymbol{O} \neq \emptyset$ indicates that a collision is likely to occur in this segment of the path and $\frac{\boldsymbol{V}_g}{|\boldsymbol{V}_g|} \neq \frac{\boldsymbol{p}_{i+1}-\boldsymbol{p}_i}{|\boldsymbol{p}_{i+1}-\boldsymbol{p}_i|}$ means that the controller cannot keep the direction of the vehicle moving in the same direction as the path, which implies the counter-current at $\boldsymbol{p}_i$ is too strong for the AUV to move forward along P.

If path P is infeasible, its cost will be deemed as infinite:

$$J = t_{sum} = \begin{cases} \infty & \exists F_i = 0 \\ \sum_i^{n-1} t_i & \text{others} \end{cases}. \tag{31}$$

For clarity, the pseudo-codes of the procedure of the path evaluation is summarized in Algorithm 1.

Algorithm 1 Evaluate path using forecast maps.

1: Input path $P = \{\boldsymbol{p}_0, \boldsymbol{p}_1, \ldots, \boldsymbol{p}_n\}$.
2: Input AUV velocity V_a, forecast map series $\boldsymbol{M}_f = \{M_1, M_2, \ldots, M_N\}$ and map update interval T_s.
3: Set timer $t = 0$ and $j = 1$.
4: **for** $i = 0, 1, 2, \ldots, n-1$ **do**
5: Use M_j to obtain AUV's ground-referenced speed $\boldsymbol{V}_g = \boldsymbol{V}_a + \boldsymbol{V}_c$.
6: $t_i = \frac{|\boldsymbol{p}_{i+1}-\boldsymbol{p}_i|}{|\boldsymbol{V}_g|}$.
7: $t = t + t_i$.
8: **if** $[\boldsymbol{p}_i, \boldsymbol{p}_{i+1}] \cap \{\boldsymbol{O}, \boldsymbol{L}\} \neq \emptyset$ or $\frac{\boldsymbol{V}_g}{|\boldsymbol{V}_g|} \neq \frac{\boldsymbol{p}_{i+1}-\boldsymbol{p}_i}{|\boldsymbol{p}_{i+1}-\boldsymbol{p}_i|}$ **then**
9: $t = \infty$.
10: Break loop and jump to line 14.
11: **end if**
12: $j = [\frac{t}{T_s}] + 1$.
13: **end for**
14: **return** t.

4 Re-sensing and Path Re-planning

The forecast environment map-based planner guarantees the security and reduces energy consumption effectively by introducing prediction information. Without the prediction, the AUV will carry out unplanned maneuver when it detects an obstacle online to avoid the collision, and that will consume much unplanned energy and deteriorate the AUV's endurance dramatically.

However, Eq. 23 indicates that the prediction error increases linearly with time, and more and more areas will be marked as no-fly zone due to the forecast uncertainty, hence the reduction of the positive influence of the predictive information. Besides, the scope of the onboard sensors is limited, the AUV will approach the undetected area gradually. To further improve the energy efficiency based on the conservative path planning strategy and reduce the prediction error by the feedback mechanism, the path re-planning strategy is introduced.

4.1 Modify the Prediction by Acquiring New Measurements

If the AUV re-senses the environment during the movement, the accumulated prediction error can be effectively reduced. Due to the battery limit, the sensing system equipped does not keep working all the time: after a period of work, the sensing system will enter the standby mode until the processor issues a re-planning instruction.

After being awakened from the standby mode, the detecting sonar and H-ADCP restore sensing the environment, and the new measurements will be sent to the CPU. The state estimation $\hat{\boldsymbol{x}}(k+N|k+N)$ will be updated according to the new measurement $\boldsymbol{z}(k+N)$:

$$\begin{aligned} \hat{\boldsymbol{x}}(k+N|k+N) = \hat{\boldsymbol{x}}(k+N|k) + \boldsymbol{K}(k+N) \\ \times \left[\boldsymbol{z}(k+N) - \boldsymbol{H}(k+N)\hat{\boldsymbol{x}}(k+N|k)\right] \end{aligned} \tag{32}$$

where $\hat{\boldsymbol{x}}(k+N|k)$ is the N-step optimal prediction obtained at time k and $\boldsymbol{K}(k+N)$ is Kalman gain derived by

$$\begin{aligned} \boldsymbol{K}(k+N) = \boldsymbol{P}(k+N|k)\boldsymbol{H}^T(k+N) \\ \times \left[\boldsymbol{H}(k+N)\boldsymbol{P}(k+N|k)\boldsymbol{H}^T(k+N) + \boldsymbol{R}(k)\right]^{-1}. \end{aligned} \tag{33}$$

Then the state estimation and prediction can be obtained by KF.

This process is equivalent to giving KF the initial value with a large error. The efficient performance of KF enables the state estimation to converge quickly. This operation is illustrated in Fig. 6, where the stars indicate the real and predicted positions of the obstacle, and the circles indicate the collision boundary defined by the position with uncertainty.

4.2 Path Re-planning with Modified Prediction

The forecast map-based path planning has taken the dynamic of the ocean current and obstacles into account.

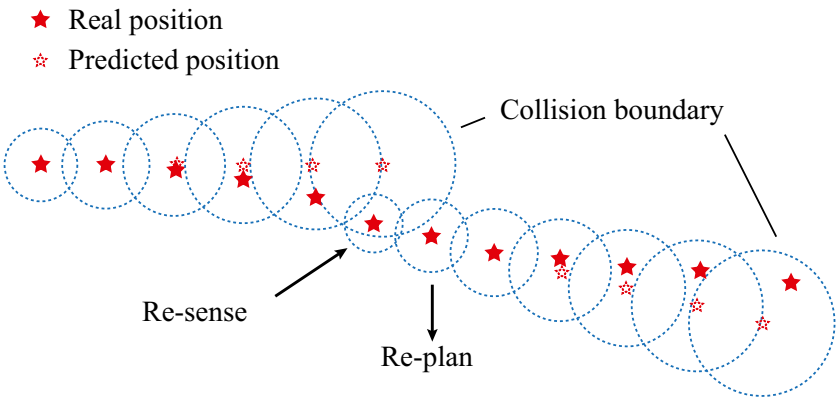

Fig. 6 Re-sensing for prediction error reduction

Based on this, the path re-planning by re-sensing the environment can effectively correct the deterioration of path planning optimality.

Given the continuity and slowness of the environment's changes, the path planning problem in the new circle is similar to the previous one, thus it is rational to deem that the new optimal path is most likely to be found near the previous path [37]. The first generation $\boldsymbol{C} = \{C_i | 1 \leq i \leq n\}$ in the re-planning is initialized by

$$C_i = \begin{cases} C_i^p & i < \lambda n \\ C_{new} & \text{others} \end{cases} \tag{34}$$

where n is population size, $0 < \lambda < 1$ is the reused rate and C_i^p is the individual with the i-th largest fitness in the previous generation $\boldsymbol{C}^p = \{C_i^p | 1 \leq i \leq n\}$. The new individuals are randomly generated according to Section 3.1.1.

When the re-prediction is completed after the re-sensing, a new planning process will be performed based on the new generation. A new optimal path P_{new}^* from the current position to the destination will be obtained, and the rest of the previous planned path P^* will be discarded. The AUV will follow P_{new}^* to complete the rest journey until the re-sensing and re-planning are performed again.

Obviously, more frequent re-planning results in more accuracy and consumes more energy. To decide when to carry out the re-planning, a simple and convenient way is to set a re-planning interval. Besides that, a more flexible re-planning trigger mechanism can be adopted. As mentioned before, the error covariance matrix $\boldsymbol{P}(k+N|k)$ describes the uncertainty of the predicted state, thus it can be used to determine when to perform the re-planning. The re-planning threshold is set to S on the need of the prediction accuracy. The re-planning will be performed when the trace of the error covariance matrix satisfies

$$\mathrm{tr}\boldsymbol{P}(k+i|k) > S \tag{35}$$

where $i = 1, 2, \ldots, N$ and N is the maximum prediction step. After the re-planning, the AUV will follow the new path and the planner will wait for the next re-planning.

5 Simulation Results

To verify the effectiveness and superiority of the proposed path planning method, simulations are performed in Matlab R2017b under Windows 10 on a PC with Intel i7-8700 CPU, 16 GB of RAM. Four sets of simulations are designed to explore the performance of our path planning method, and it is compared with traditional path planners which do not take the dynamic environment into consideration. In the first simulation, the AUV moves in a dynamic current field. The main purpose is to take full use of the ocean energy to shorten the travel time. In the second simulation scenario, moving obstacles exist and the reliability and robustness of the proposed algorithm are tested. In addition to considering energy consumption, the AUV should also avoid temporary maneuvers that are executed to avoid collisions. Subsequently, the re-planning mechanism is introduced in the third test. Lastly, a real map is used to test the effectiveness of the entire path planning strategy.

The simulations are based on the torpedo type AUV THB050R produced by Tianhe Maritime, as shown in Fig. 7. The well-expandable AUV can be equipped with multiple different types of sensors in the form of external hangers and cabins. The AUV's water-referenced velocity is set to $1m/s$, and its minimum turning radius is 15 meters. In the simulation tests, the 2D $500m \times 500m$ mission region is divided into 100×100 grid. The spatiotemporal current field is composed of four dynamic vortexes. The current velocity is limited to less than $0.6m/s$, and the vortexes move in random different directions at the speed of $0.1m/s$. Except for the first simulation scenario, several moving obstacles exist in the mission region, and the current field is updated every 50 seconds. The parameters of DE are listed in Table 1.

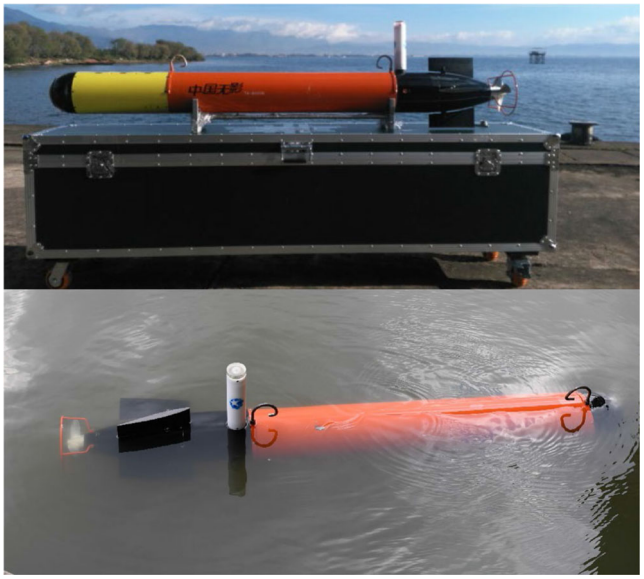

Fig. 7 Torpedo type AUV: TH-B050R

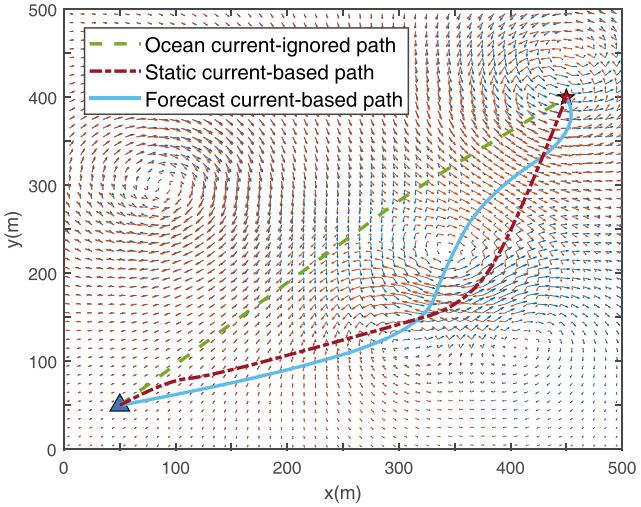

Fig. 8 Optimal paths given by OCIP, SCP, and FCP

5.1 Energy-saving Performance in Spatiotemporal Current Field

In this simulation case, we study the performance of the path planner when the AUV moves in a spatiotemporal current field. The AUV departs from $(50, 50)$ (marked with a triangle) and the destination is $(450, 400)$ (marked with a star). Before the departure, the current field is sensed by the H-ADCP for several intervals, and that guarantees the convergence of the current estimation. The observation errors of each vortex center, strength, and radius are respectively $Q_{\boldsymbol{r}_0} \sim \mathcal{N}(0, 1)$, $Q_\Gamma \sim (0, 0.5)$, and $Q_\delta \sim (0, 0.5)$. The KF-based multi-step optimal prediction will be performed, and the forecast maps are used by the DE-based planner to generate the optimal path for the AUV to follow. 30 Monte Carlo (MC) experiments are performed.

Traditionally, the ocean current is ignored or only the static current information is used to evaluate possible paths. Figure 8 shows the paths obtained by the ocean current-ignored planner (OCIP) [38], the static current-based planner (SCP) [15], and the proposed forecast current-based planner (FCP) in one typical experiment. The current fields at $t = 0$ and $t = 600s$ are represented by two sets of arrows that represent the intensity and direction simultaneously. The average of the MC experiments result is listed in Table 2. The expected time cost refers to the time that a planner expects the AUV to spend on the given path, while the execution time cost refers to the actual time spent in the experiments. The MC experiments result shows that the proposed FCP has respectively saved 10.9% and 6.6% time compared with the OCIP and the SCP. It can be observed that when the AUV departs, the current field in the lower right of Fig. 8 forms an area that is downstream for the AUV's traveling. The static current-based planner tends to utilize the current to compress the energy cost. However, the dynamics of ocean current restricts this downstream current from lasting, and the current becomes unfavorable for the AUV's movement later. In contrast, the designed FCP considers the dynamic of ocean current and effectively improves the energy efficiency.

Table 1 Parameter setting of DE

Population Size	Iterations	Scaling Factor	Crossover Rate	Control Points
50	100	0.5	0.6	5

5.2 Robustness Facing Dynamic Obstacles

The performance of our path planning methods is explored when dynamic obstacles exist in the mission region. Based on the simulation set in the previous case, the static no-fly zone exists in the mission area, together with three obstacles moving in CV mode at the speed of $0.08, 0.08, 0.06m/s$, respectively. In addition to taking full advantage of ocean currents to save energy, the AUV should keep the safety distance from obstacles at all times. Therefore, the real-time no-fly zone is determined by comprehensively considering

Table 2 Planning result of different planning methods in spatiotemporal current field

	OCIP	SCP	FCP
Expected Time Cost (s)	532.0	540.8	571.7
Execution Time Cost (s)	641.2	612.1	571.6
CPU Time (s)	1.63	2.59	2.96

the safety distance and the uncertainty of obstacles' position.

Figure 9 presents the comparison of the results of the two path planner. The static environment-based planner (SEP) [12] plans the path based on the environmental information that the vehicle detects at the time of departure, while the proposed predicted environment-based planner (FEP) takes the dynamic of the environment into consideration additionally. Significant differences exist between the two paths: the SEP path shifts to the right in the middle stage in order to rely more efficiently on the current. However, on account of the lack of estimation of obstacles' future position, there is a high probability of the collision at the position marked by a hexagram. By contrast, the AUV following the FEP path avoids possible dangers by predicting the location of obstacles in advance.

The online collision avoidance system keeps working during the entire AUV movement to ensure safety. When an obstacle is detected in front of the AUV, maneuvers will be performed to avoid the collision. However, the temporary maneuver requires an emergency brake and yaw, which will consume much unplanned energy. Besides, not every circumvention will be successful. Therefore, the reliability of planners can be reflected by the probability of the circumvention. In our experiments, if an obstacle appears within the safe distance from the AUV during the operation, the AUV will be considered to be threatened and it will need to perform a maneuver. Hence, a greater safety distance means a smaller chance of a collision. Due to the uncertainty in the location of obstacles, different safety distances are set and the reliability of the paths given by the SEP and the FEP are tested in 100 MC experiments, and the result is presented by Fig. 10. Compared with the FEP which guarantees security almost all the time, the path generated by the SEP results in the risk of 10% at the safety distance of $2m$. That means the AUV encounters at least one collision in 10% of the experiments, and the probability of risk increases with the threshold for risk determination (safety distance). We can conclude that the proposed path planning method is more likely to avoid the circumstance in which the AUV deviates the established motion plan, or even be damaged in an accident.

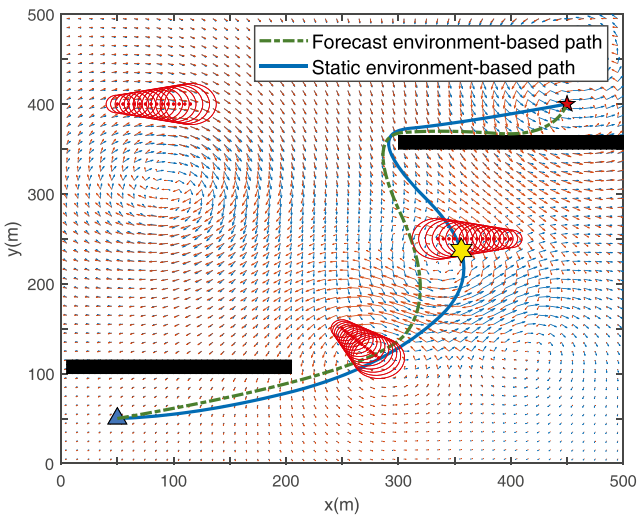

Fig. 9 Optimal paths in mission region with spatiotemporal current and dynamic obstacles

5.3 Path Planning with Re-planning Mechanism

In this part, path re-planning with environment re-sensing is introduced to further improve the performance of the path planner. During the AUV's movement, the onboard sensing system will be turned on whenever the path re-planning is triggered, and the future state of the spatiotemporal current field and dynamic obstacles will be re-predicted according to the new information.

Three moving obstacles exist in the AUV's working area. The previous discussion implies that the proposed path planner tends to give a more conservative but safer result. The re-planning mechanism expands the solution space on the promise that the AUV's safety is ensured. The initial path is generated based on the prediction of the environment before the AUV's departure. The uncertainty of obstacle prediction increases with time, that is, the area where the obstacles are likely to appear is becoming larger and larger. For safety, the planner leads to AUV to avoid the no-fly zone occupied by the risk area. Meanwhile, the feasible solution space is largely compressed, which limits the further optimization of the energy consumption. To push the limit caused by the conservative strategy, the sensing system will be turned on for a while during the movement, and the path re-planning will be performed sequentially based on the new environmental information.

Figure 11 presents the paths when the re-planning is not performed, performed once, and twice. The positions of the two re-plannings are marked in the figure. The AUV moves along a new path after a re-planning is performed. It can be seen that the two re-planned path is visibly different from

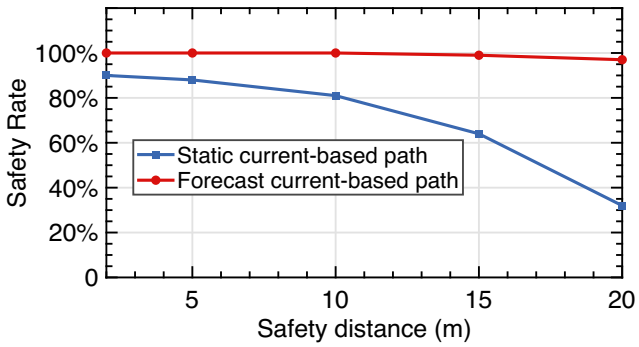

Fig. 10 Safety rate under different path planning strategies

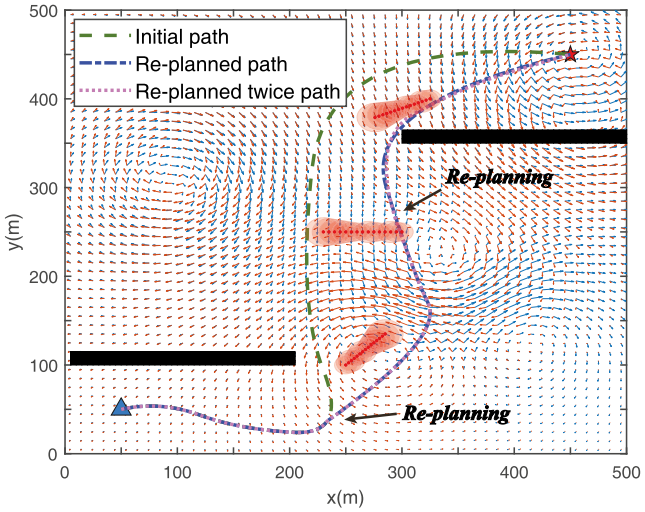

Fig. 11 The initial and re-planned paths

the initial one: the AUV does not choose the open area on the left but moves through the gap between the obstacles and the land when the safety is confirmed. Additionally, the last re-planning path almost coincides with the previous one, and this indicates that in the simulation scenario, the new information obtained from the last re-sensing is of limited help to improve the optimality of the planning result.

The expected and tested results of time consumption in 50 Monte Carlo experiments are shown in Fig. 12, where the central mark, bottom and top edges mark on each box indicate the median, the 25th and 75th percentiles, respectively, and the whiskers extend to the most extreme data points not considered outliers, while the outliers are noted individually by the 'o' symbol. The expected time cost is the running time estimated by the planner, and the tested time cost is the average of 30 tests, in which the variation of the environment is random. The average tested time costs of the initial and re-planned path are 770.7s and 718.3s, respectively. The proposed re-sensing and re-planning mechanism helps the AUV save 6.8% energy at the cost of tripling the computation cost compared with the no-re-planning planner.

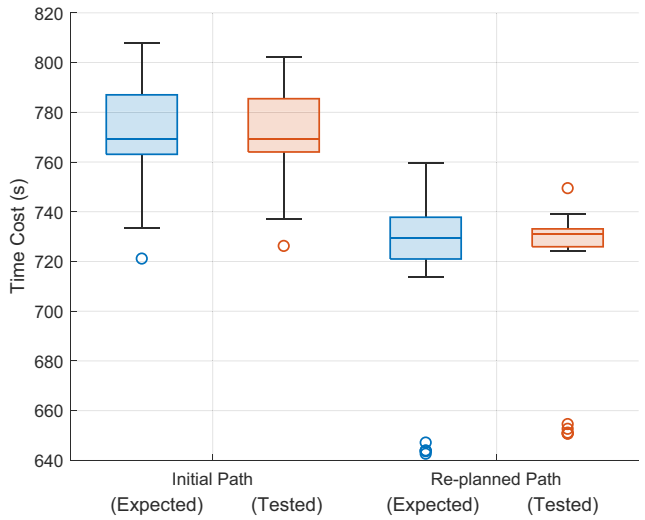

Fig. 12 Improve performance by re-planning: costs in simulation and execution

5.4 Path Planning in Complex Actual Environment

In this case, the proposed planner is tested in a real scenario. In the cage farming area of Luxi Island, Zhejiang, China, nodes in the sensor network transmit the water quality monitoring data to the central node [39], and an AUV equipped with communication system is ordered to approach and retrieve data from the center node. The starting and ending points are marked in Fig. 13, and the AUV working area is presented. The vehicle needs to avoid fixed obstacles (land, fish cages, and cultivation facilities) and moving obstacles using based on the onboard sensing system, and it should reach the destination with the lowest possible energy consumption. The FEP with the re-planning mechanism is tested in this experiment. The SEP only based on static environmental information is tested as a contrast. The AUV detects obstacles and avoids collisions in real-time during the operation, additional 30s will be added into the total time cost, and the path will be re-planned if an unplanned maneuver occurs.

As shown in Fig. 14, the static map is loaded prior to the launch of the AUV, and the spaces occupied by static obstacles are marked as the no-fly zone. The solid curve

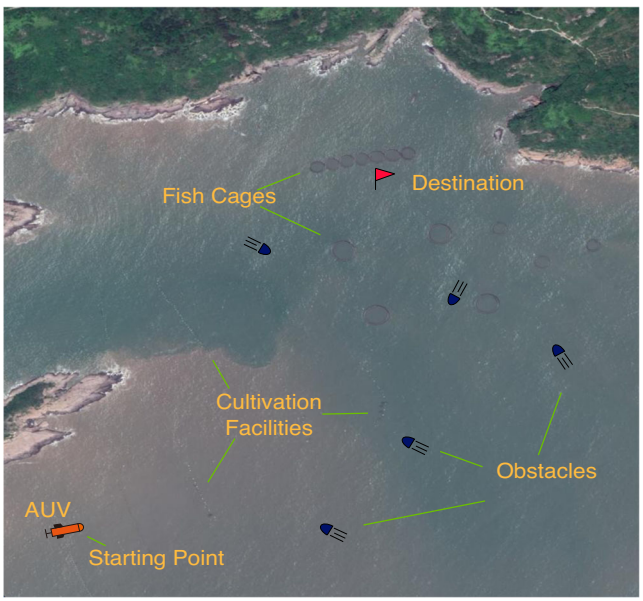

Fig. 13 Results for the mission in Luxi island cage area given by path planners

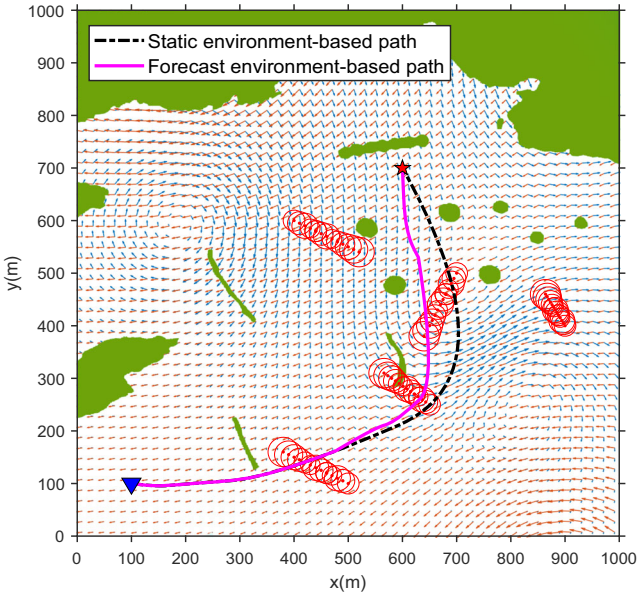

Fig. 14 Results for the mission in Luxi island cage area given by path planners

represents the FEP path. By following this path, the AUV successfully avoids collisions and reaches the destination safely. The dash-dot curve represents the path given by the SEP. As the AUV following this path travels to the location of about (600, 200), an obstacle in front of it is detected, and the AUV immediately adjusts its course to the southeast direction to avoid the collision. When the AUV is safe, the current position is used as the starting point to re-plan the new path for the AUV to finish its journey. The AUV employing SEP has also reached the destination, but there is an emergency evasion on its way. The static environment-based planner and the proposed planner are tested in 10 different environments where the states of the five moving obstacles and vortexes are generated randomly. The result of the 50 MC tests is shown in Fig. 15. The average execution times are 1135.7*s* and 1190.5*s* respectively, and the proposed path planner helps the AUV save about 4.6% of the running time.

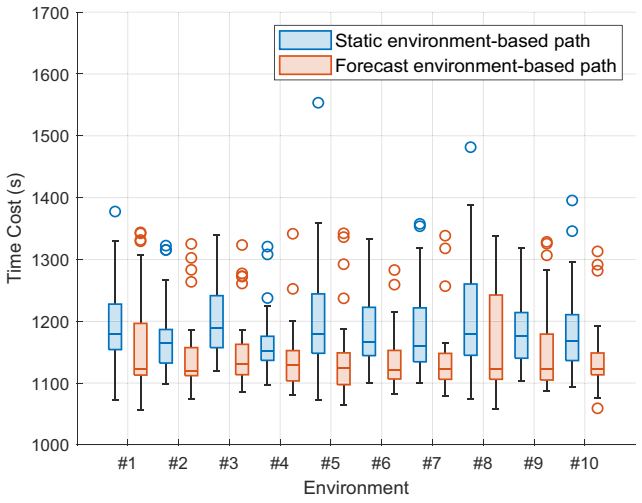

Fig. 15 Execution time of path planners in MC experiments

6 Conclusion

In this paper, we propose a novel path planning method for the AUV working in small-scale time-varying ocean environment. The proposed method predicts the future of ocean current and dynamic obstacles based on the measurements obtained by onboard sensors. The DE algorithm is employed to generate candidate paths, and the environment prediction is used to evaluate these paths to select the optimal one. The re-planning strategy is adopted to correct the errors online. The path planner is tested in multiple simulation scenarios, which takes land, spatiotemporal ocean current, static and dynamic obstacles into consideration. The results suggest that the planner helps the AUV to take full advantage of the ocean current and avoid collision efficiently, thereby reducing at least 4.6% travel time compared with the existing methods.

Future work involves designing a complete vehicle path planning framework that enables the vehicle to perform a series of tasks, and 3D environment prediction algorithms will be proposed. Additionally, hardware design is required to integrate multiple sensing devices on the AUV.

Author Contributions J. Zhang and M. Liu contributed to the design and implementation of the research, the analysis of the results and the writing of the first draft of the manuscript. S. Zhang and R. Zheng commented on previous versions of the manuscript. All authors read and approved the final manuscript.

Funding This work was supported by the NSFC-Zhejiang Joint Fund for the Integration of Industrialization and Informatization under Grants U1709203, U1809212 and U1909206, the Zhejiang Provincial Natural Science Foundation of China under grant LZ19F030002, the Key Research and Development Program of Zhejiang Province under Grant 2019C03109, and the NSFC under Grant 62088102.

Code Availability The MATLAB codes used and analyzed during the study are available from the first author on reasonable request.

Declarations

Competing interests The authors declare that they have no conflict of interest.

References

1. Li, D., Wang, P., Du, L.: Path planning technologies for autonomous underwater vehicles-a review. IEEE Access **7**, 9745–9768 (2019)
2. Perera, L.P., Carvalho, J., Soares, C.G.: Intelligent ocean navigation and fuzzy-Bayesian decision/action formulation. IEEE J. Ocean. Eng. **37**(2), 204–219 (2012)
3. Soulignac, M.: Feasible and optimal path planning in strong current fields. IEEE Trans. Robot. **27**(1), 89–98 (2010)
4. Zhang, H.H., Gong, L., Chen, T., Wang, L., Zhang, X.: Global path planning methods of UUV in coastal environment. In: Proc. IEEE International Conference on Mechatronics and Automation (ICMA), pp. 1018–1023, Harbin, China (2016)
5. Yu, H., Wang, Y.: Multi-objective AUV path planning in large complex battlefield environments. In: Proc. International Symposium on Computational Intelligence and Design (ISCID), vol. 2, pp. 345–348, Hangzhou, China (2014)
6. Lolla, T., Ueckermann, M.P., Yiğit, K., Haley, P.J., Lermusiaux, P.F.: Path planning in time dependent flow fields using level set methods. In: Proc. IEEE International Conference on Robotics and Automation (ICRA), pp. 166–173, Saint Paul, MN, USA (2012)
7. Ammar, A., Bennaceur, H., Châari, I., Koubâa, A., Alajlan, M.: Relaxed dijkstra and A* with linear complexity for robot path planning problems in large-scale grid environments. Soft Comput. **20**(10), 4149–4171 (2016)
8. Hernández, J.D., Istenič, K., Gracias, N., Palomeras, N., Campos, R., Vidal, E., Garcia, R., Carreras, M.: Autonomous underwater navigation and optical mapping in unknown natural environments. Sensors **16**(8), 1174 (2016)
9. Janson, L., Ichter, B., Pavone, M.: Deterministic sampling-based motion planning: Optimality, complexity, and performance. Int. J. Robot. Res. **37**(1), 46–61 (2018)
10. Xiong, C., Lu, D., Zeng, Z., Lian, L., Yu, C.: Path planning of multiple unmanned marine vehicles for adaptive ocean sampling using elite group-based evolutionary algorithms. J. Intell. Robot. Syst. pp. 1–15 (2020)
11. Wang, X., Yao, X., Zhang, L.: Path planning under constraints and path following control of autonomous underwater vehicle with dynamical uncertainties and wave disturbances. J. Intell. Robot. Syst. pp 1–18 (2020)
12. Zeng, Z., Zhou, H., Lian, L.: Exploiting ocean energy for improved AUV persistent presence: path planning based on spatiotemporal current forecasts. J. Mar. Sci. Technol. **25**(1), 26–47 (2020)
13. Perez-Carabaza, S., Besada-Portas, E., Lopez-Orozco, J.A., Jesus, M.: Ant colony optimization for multi-UAV minimum time search in uncertain domains. Appl. Soft Comput. **62**, 789–806 (2018)
14. MahmoudZadeh, S., Powers, D.M., Yazdani, A.M.: A novel efficient task-assign route planning method for AUV guidance in a dynamic cluttered environment. In: Proc. IEEE Congress on Evolutionary Computation (CEC), pp. 678–684, Vancouver, BC, Canada (2016)
15. Mahmoudzadeh, S., Powers, D.M.W., Atyabi, A.: UUV's hierarchical DE-based motion planning in a semi dynamic underwater wireless sensor network. IEEE Trans. Cybern. **49**(8), 2992–3005 (2019)
16. Tsai, C.C., Huang, H.C., Chan, C.K.: Parallel elite genetic algorithm and its application to global path planning for autonomous robot navigation. IEEE Trans. Ind. Electron. **58**(10), 4813–4821 (2011)
17. Petres, C., Pailhas, Y., Patron, P., Petillot, Y., Evans, J., Lane, D.: Path planning for autonomous underwater vehicles. IEEE Trans. Robot. **23**(2), 331–341 (2007)
18. Isern-González, J., Hernández-Sosa, D., Fernández-Perdomo, E., Cabrera-Gámez, J., Domínguez-Brito, A.C., Prieto-Marañón, V.: Path planning for underwater gliders using iterative optimization. In: Proc. IEEE International Conference on Robotics and Automation (ICRA), pp. 1538–1543, Shanghai, China (2011)
19. Kim, K., Ura, T.: Towards a new strategy for AUV navigation in sea currents: A quasi-optimal approach. In: Proc. IEEE Symposium on Underwater Technology and Workshop on Scientific Use of Submarine Cables and Related Technologies (SSC), pp. 1–10, Tokyo, Japan (2011)
20. Barron, C.N., Kara, A.B., Martin, P.J., Rhodes, R.C., Smedstad, L.F.: Formulation, implementation and examination of vertical coordinate choices in the Global Navy Coastal Ocean Model (NCOM). Ocean Model. **11**(3-4), 347–375 (2006)
21. Garau, B., Alvarez, A., Oliver, G.: AUV navigation through turbulent ocean environments supported by onboard H-ADCP. In: Proc. IEEE International Conference on Robotics and Automation (ICRA), pp. 3556–3561, Orlando, FL, USA (2006)
22. Lamb, H.: Hydrodynamics. Cambridge University Press, Cambridge (1993)
23. Karmozdi, A., Hashemi, M., Salarieh, H., Alasty, A.: INS-DVL navigation improvement using rotational motion dynamic model of AUV. IEEE Sensors J. **20**(23), 14329–14336 (2020)
24. Lammas, A.K., Sammut, K., He, F.: A 6 DoF navigation algorithm for autonomous underwater vehicles. In: Proc. OCEANS 2007-Europe, pp. 1–6, Aberdeen, UK (2007)
25. Pereira, A.A., Binney, J., Hollinger, G.A., Sukhatme, G.S.: Risk-aware path planning for autonomous underwater vehicles using predictive ocean models. J.Field Robot. **30**(5), 741–762 (2013)
26. Gonzalez, J.P., Stentz, A.: Planning with uncertainty in position an optimal and efficient planner. In: Proc. IEEE/RSJ International Conference on Intelligent Robots and Systems (IROS), pp. 2435–2442, Edmonton, Alta., Canada (2005)
27. Pak, J.M., Kim, P.S., You, S.H., Lee, S.S., Song, M.K.: Extended least square unbiased FIR filter for target tracking using the constant velocity motion model. Int. J. Control Autom Syst. **15**(2), 947–951 (2017)
28. Chen, H.Y., Liu, M.Q., Zhang, S.L.: Energy-efficient localization and target tracking via underwater mobile sensor networks. Front Inform Technol Electron Eng **19**(8), 999–1012 (2018)
29. Zeng, Z., Sammut, K., Lian, L., He, F., Lammas, A., Tang, Y.: A comparison of optimization techniques for AUV path planning in environments with ocean currents. Robot. Auton. Syst. **82**, 61–72 (2016)
30. Das, S., Mullick, S.S., Suganthan, P.N.: Recent advances in differential evolution–an updated survey. Swarm Evol Comput **27**, 1–30 (2016)
31. Prautzsch, H., Boehm, W., Paluszny, M.: Bézier and B-spline Techniques. Springer Science & Business Media, Berlin (2013)
32. Lo, K.W., Ferguson, B.G.: Automatic detection and tracking of a small surface watercraft in shallow water using a high-frequency active sonar. IEEE Trans. Aerosp. Electron. Syst. **40**(4), 1377–1388 (2004)
33. Bar-Shalom, Y., Li, X.R., Kirubarajan, T.: Estimation with Applications to Tracking and Navigation: Theory Algorithms and Software. John Wiley & Sons, Germany (2004)
34. Gauvrit, H., Le Cadre, J.P., Jauffret, C.: A formulation of multitarget tracking as an incomplete data problem. IEEE Trans. Aerosp. Electron. Syst. **33**(4), 1242–1257 (1997)
35. Hu, Z., Leung, H., Blanchette, M.: Statistical performance analysis of track initiation techniques. IEEE Trans. Signal Process. **45**(2), 445–456 (1997)
36. Han, C., Zhu, H., Duan, Z.: Multi-source Information Fusion. Tsinghua University Press, Beijing (2010)

37. Zeng, Z., Sammut, K., Lammas, A., He, F., Tang, Y.: Efficient path re-planning for AUVs operating in spatiotemporal currents. Intell. Robot. Syst. **79**(1), 135–153 (2015)
38. Li, J.J., Zhang, R.B., Yu, Y.: Research on route obstacle avoidance task planning based on differential evolution algorithm for auv. In: International Conference in Swarm Intelligence. Springer International Publishing, Cham (2014)
39. Wang, J., Shi, W., Xu, L., Zhou, L., Niu, Q., Liu, J.: Design of optical-acoustic hybrid underwater wireless sensor network. J. Netw. Comput. Appl. **92**, 59–67 (2017)

Jiaxin Zhang received the B.E. degree in automation from Zhejiang University, Hangzhou, China, in 2014. He is currently pursuing the Ph.D. degree in control theory and control engineering with Zhejiang University, Hangzhou.

His research interests include AUV path planning and multi-AUV cooperation.

Meiqin Liu received the B. E. and Ph.D. degrees in control theory and control engineering from Central South University, Changsha, China, in 1994 and 1999, respectively.

She was a Post-Doctoral Research Fellow with the Huazhong University of Science and Technology, Wuhan, China, from 1999 to 2001. She was a Visiting Scholar with the University of New Orleans, New Orleans, LA, USA, from 2008 to 2009. She was a Professor with the College of Electrical Engineering, Zhejiang University, Hangzhou, China, from 2001 to 2021. She is currently a Professor with the Institute of Artificial Intelligence and Robotics, Xi'an Jiaotong University, Xi'an, China, and also with the State Key Laboratory of Industrial Control Technology, Zhejiang University, Hangzhou, China. She has authored more than 200 papers in major journals and international conferences. She has led 16 national or provincial or ministerial projects in the last 5 years, including 9 projects funded by the National Natural Science Foundation of China (NSFC). Her work was supported by the Zhejiang Provincial Natural Science Fund for Distinguished Young Scholars in 2010, and by the National Science Fund for Excellent Young Scholars of China in 2012, respectively. She has won a second prize of Science and Technology Award of Zhejiang Province in 2013, and a first prize of Natural Science Award of Chinese Association of Automation in 2019, respectively. Her current research interests include theory and application of artificial intelligence, multi-sensor networks, information fusion, and unmanned undersea systems.

Senlin Zhang received the B.E. degree in control theory and control engineering from the Wuhan University of Technology, Wuhan, China, and the M.E. degree in control theory and control engineering from Zhejiang University, Hangzhou, China, in 1984 and 1991, respectively. He is currently a Professor with the College of Electrical Engineering, Zhejiang University, Hangzhou. He has authored more than 100 papers in major journals and international conferences. His current research interests include unmanned undersea systems, intelligent systems, and multi-sensor networks.

Ronghao Zheng received the B.S. degree in electrical engineering and the M.S. degree in control theory and control engineering from Zhejiang University, Hangzhou, China, in 2007 and 2010, respectively, and the Ph.D. degree in mechanical and biomedical engineering from the City University of Hong Kong, Hong Kong, in 2014.

He is currently with the College of Electrical Engineering, Zhejiang University. His research interests include distributed algorithms and control, especially the coordination of networked mobile robot teams with applications in automated systems and security.